Geochemical Perspectives Letters

Correlative microspectroscopy of biogenic fabrics in Proterozoic silicified stromatolites

K. Hickman-Lewis, B. Cavalazzi, W. Montgomery

Supplementary Information

The Supplementary Information includes:

- Experimental Protocols
- Tables S-1 and S-2
- Figures S-1 to S-14
- Supplementary Information References

Experimental Protocols

1. Samples and subsamples

The samples utilised for this research are part of the Martin Brasier Collection housed at the Oxford University Museum of Natural History, Oxford, United Kingdom. Six thin sections were imaged and studied using optical microscopy, from which three thin sections were chosen for further analysis based on the presence of mesoscale organic-rich laminations within. Organic-rich laminations were selected as regions of interest for geochemical study using SEM-EDX and Raman and FTIR microspectroscopy.

2. Optical microscopy

Transmitted and cross-polarised light optical photomicrographs were acquired using Leica Axio Scope.A1 (OUMNH, Oxford) and Olympus BX63 (NHM, London) microscopes. Images were acquired at magnifications between 20× and 1000× and captured using ZEN and CellSens software.

3. Scanning electron microscopy and energy-dispersive X-ray spectroscopy

SEM-EDS was undertaken using a JEOL JSM-IT 500 variable pressure SEM equipped with an Oxford Instruments X-Max EDS detector at the Natural History Museum (NHM), London. EDS maps were acquired at an accelerating voltage of 15 kV for 120 minutes. EDS spot analyses were acquired at an accelerating voltage of 15 kV for 180 s. Data were acquired and processed using AZtec software (Oxford Instruments).

4. Raman microspectroscopy

Raman maps were acquired using a WITec Confocal Raman microscope alpha300R system at the BiGeA Raman Laboratory, Università di Bologna. The Raman signal was collected using a 100× (numerical aperture of 0.90) objective (Nikon, Tokyo, Japan) and an average laser intensity of 5 mW at a depth beneath the thin section surface of 5 µm. Prior to analysis, samples were cleaned with isopropyl alcohol then with ultra-pure water. Scans were performed using a frequency-doubled Nd-YAG laser (Newport, Evry, France) providing excitation at a wavelength of 532 nm perpendicular to the sample surface to acquire confocal 2D (*x*-*y*) Raman maps. Data acquisition, evaluation and processing were performed using the WITec Project Management and Image Project Plus software suite.

Spectral deconvolution and Raman geothermometry was conducted using the carbonaceous material-based geothermometers developed by Beyssac *et al.* (2002) and Kouketsu *et al.* (2014). The Raman signal was again collected using a 100× (numerical aperture of 0.90) objective (Nikon, Tokyo, Japan) and an average laser intensity of 5 mW at a depth beneath the thin section surface of 5 µm. Peak metamorphic temperatures were determined as follows:

1) $T = -445 \times R2 + 641$ (Beyssac *et al.*, 2002),
2) $T = -2.15 \times (\text{FWHM-D1}) + 478$ (Kouketsu *et al.*, 2014),
3) $T = -6.78 \times (\text{FWHM-D2}) + 535$ (Kouketsu *et al.*, 2014),

where FWHM-D1 and FWHM-D2 denote the full width half maxima of the D1 and D2 bands, respectively. Equation 1 is valid in the temperature range 330–700 °C; Equations 2 and 3 are valid in the temperature range 165–655 °C.

5. Fourier transform infra-red (FTIR) microspectroscopy

FTIR spectral maps were obtained using a Nicolet iN10 mx FTIR microscope (ThermoFisher Scientific) at the Imaging and Analysis Centre, NHM London. The aperture was set to 50 µm × 50 µm. Maps covered the areas of interest with a grid spacing of 50 µm in both axes. Spectra were collected from 4000–675 cm^{-1} with a spectral resolution of 4 cm^{-1} using a liquid nitrogen-cooled MCT/A detector and a KBr beamsplitter. For maps, each spectrum was collected for 19.73 seconds (64 scans). A background spectrum with the same parameters was collected through air every 20 minutes.

Single spectra (reported in Fig. 4D) were acquired for 78.92 s (256 scans) with the aperture set to 50 µm × 50 µm. A background spectrum with the same parameters was collected through air prior to each single spectrum acquisition. Data were acquired and processed using OmnicPicta software (ThermoFisher Scientific).

Supplementary Tables

Table S-1 Peak thermal histories determined by Raman geothermometry.

Geothermometer	Peak temperature	Range of validity of geothermometer
$T = -445 \times R2 + 641$ (Beyssac *et al.*, 2002)	348 ± 50 °C	330–700 °C
$T = -2.15 \times (FWHM\text{-}D1) + 478$ (Kouketsu *et al.*, 2014)	346 ± 30 °C	165–655 °C
$T = -6.78 \times (FWHM\text{-}D2) + 535$ (Kouketsu *et al.*, 2014)	317 ± 50 °C	165–655 °C

Table S-2 Peak identifications in FTIR spectra. See Figure 4d for representative FTIR spectra.

Wavenumber (cm^{-1})	Designation
2500–2700	Carbonate (dolomite)
2850	Symmetrical CH_2 stretch
2870	Carbonate (dolomite?)
2895	Methyne C–H stretch (?)
2920	Asymmetrical CH_2 stretch
2940	Carbonate (dolomite)
2960	Asymmetrical CH_3 stretch
3080	Alkene =C–H stretch

Supplementary Figures

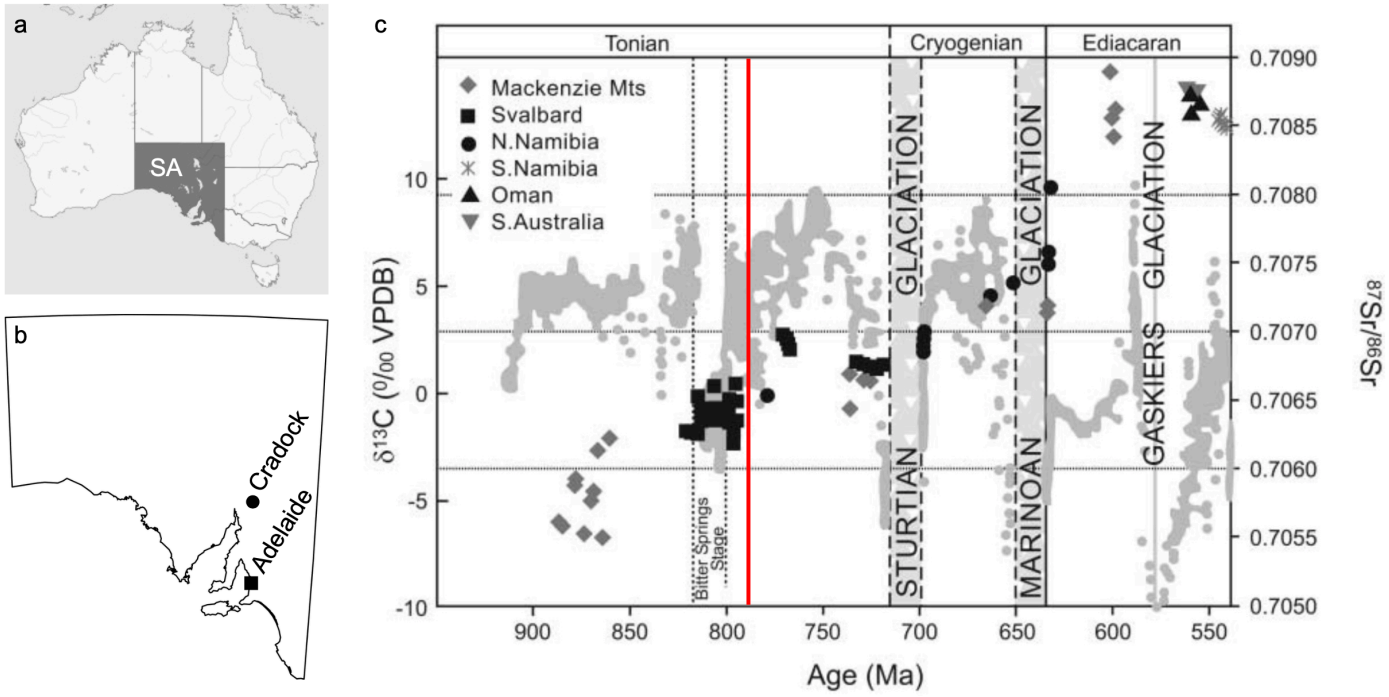

Figure S-1 Geographical and geochronological context of the Skillogalee Dolomite. **(a, b)** Locality information; the Skillogalee Dolomite samples studied were sourced from the Prince Alfred copper mine, near Cradock, South Australia (SA). **(c)** Geological timescale showing the evolution of carbonate $\delta^{13}C$ (grey symbols) and $^{87}Sr/^{86}Sr$ (black symbols) throughout the Neoproterozoic; the red line indicates the estimated age of the Skillogalee Dolomite (~790 Ma), *i.e.* during the period between the Bitter Springs Stage and the Sturtian Glaciation. Panel **(c)** is adapted from Fairchild and Kennedy (2007).

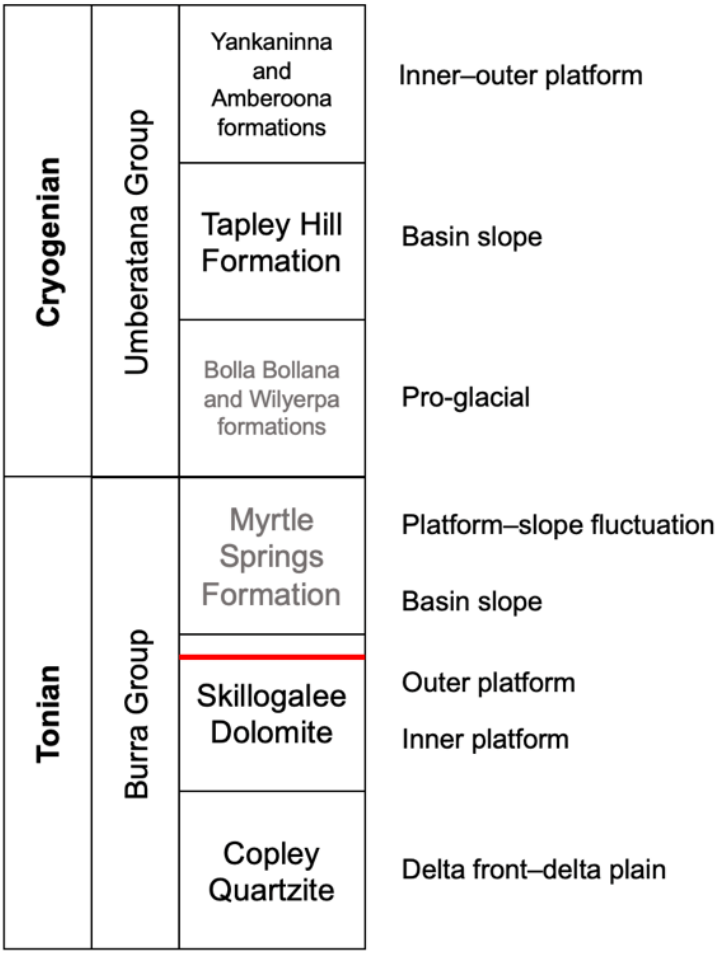

Figure S-2 Simplified stratigraphy and palaeoenvironmental reconstruction of the Tonian–Cryogenian transition in the Central Flinders Ranges. Samples were obtained from the upper Skillogalee Dolomite at the Prince Alfred copper mine near Cradock, South Australia (note that the unconformity at this locality precludes identifying the approximate stratigraphic height and horizon from which the stromatolites were sampled). Formations listed in grey text at the Tonian–Cryogenian transition do not occur at the Prince Alfred copper mine, where an unconformity separates the underlying Skillogalee Dolomite from the overlying Tapley Hill Formation. Stratigraphy adapted from Preiss (1971, 2000), Preiss *et al.* (1998), Fromhold and Wallace (2012) and Virgo *et al.* (2021). The *y*-axis is proportional to neither thickness nor time.

Figure S-3 Optical photomicrograph of thin section of Skillogalee Dolomite exhibiting silicified stromatolitic structures. Sample PM66-5. Organic-rich layers appear brown-grey in colour. Field of view is ~2 cm. Potential micro-domical biogenic features, which may represent the incipient growth of microbial domes, are arrowed.

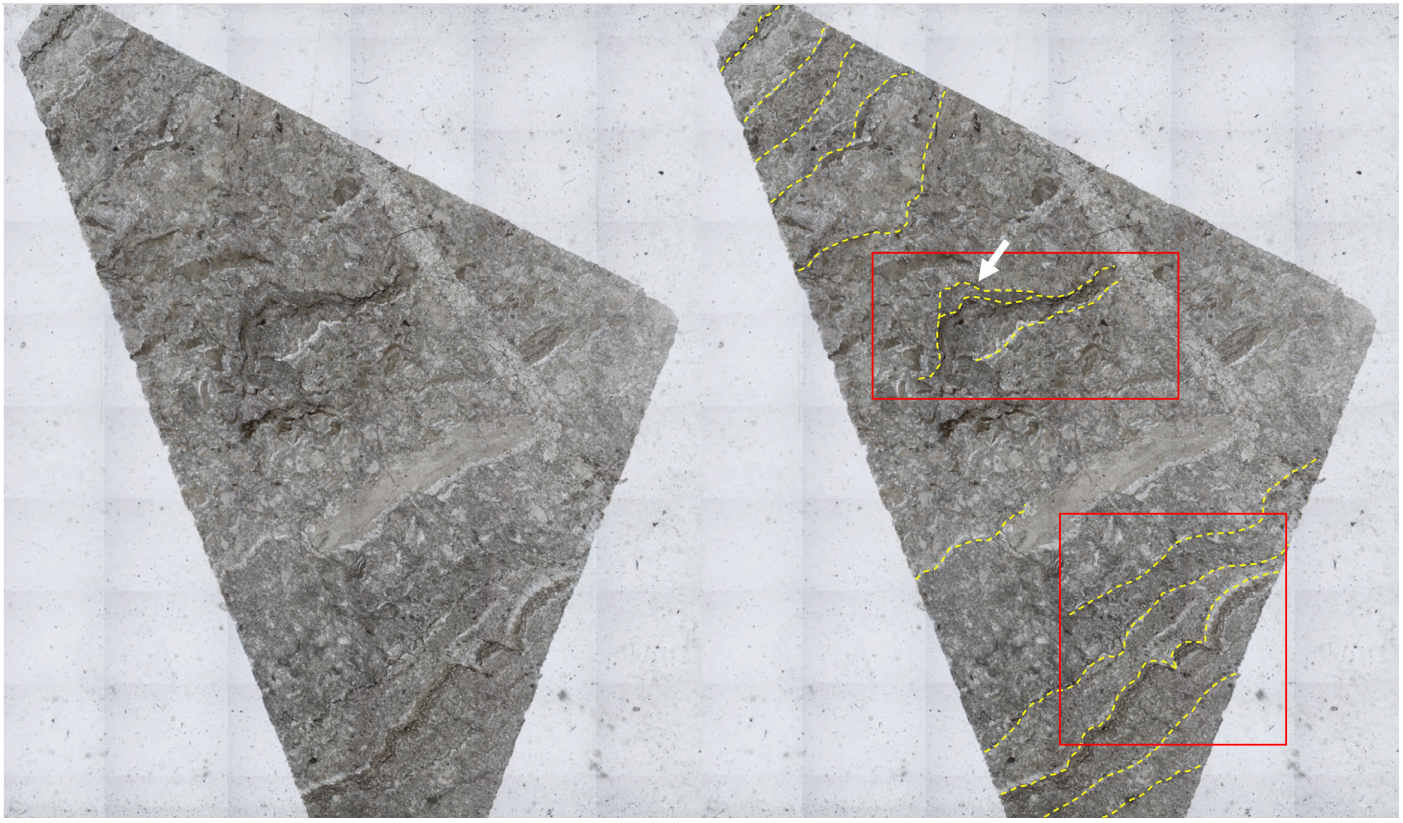

Figure S-4 Optical photomicrograph mosaics of thin section of Skillogalee Dolomite exhibiting silicified stromatolitic structures. Sample PM66-5. Organic-rich layers appear brown-grey in colour. Field of view for each photomicrograph mosaic is ~2 cm. Potential micro-domical biogenic features, which may represent the incipient growth of microbial domes, are arrowed.

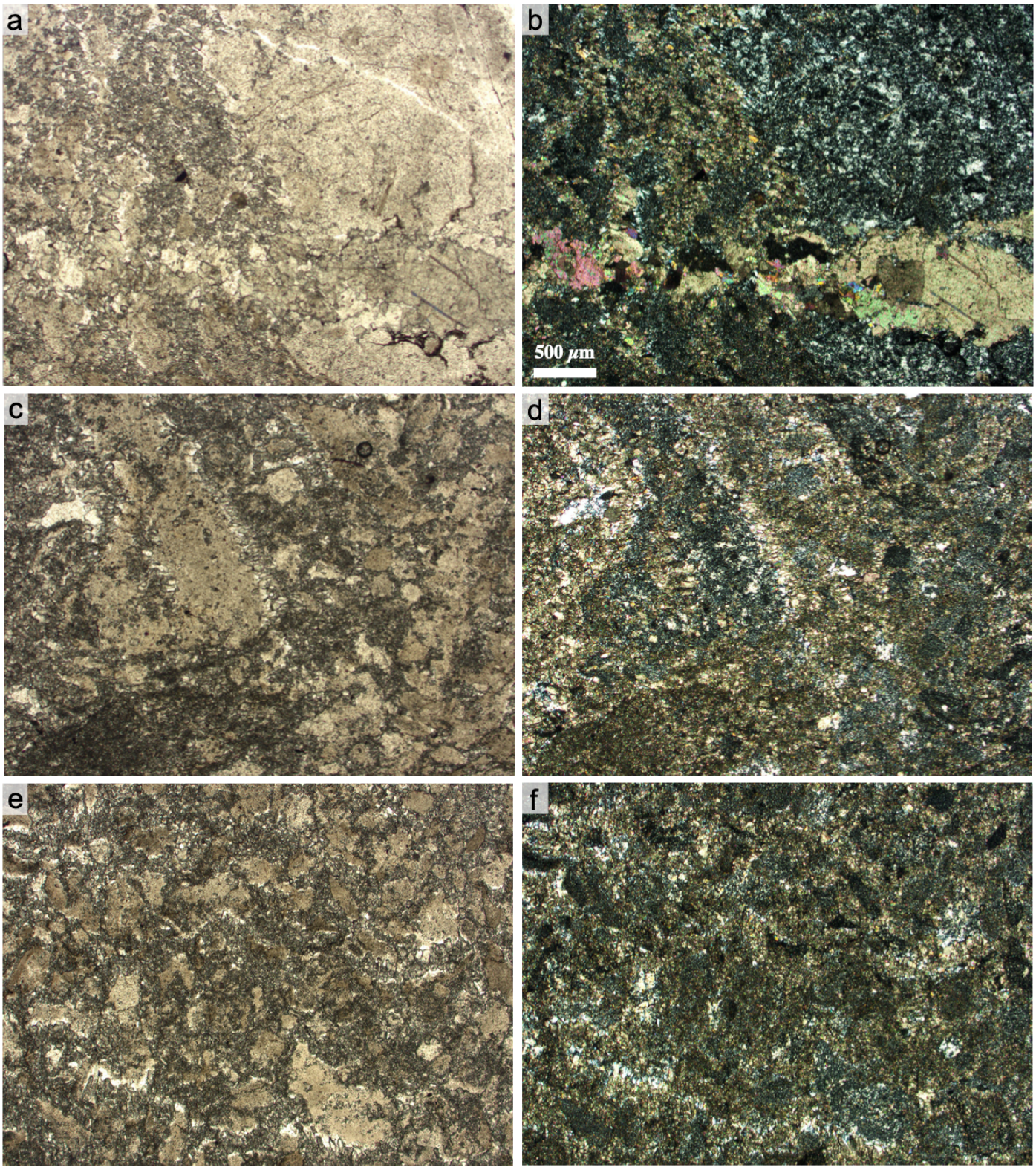

Figure S-5 Representative optical photomicrographs showing matrix carbonate fabrics (dolomite + quartz + oxides + oxyhydroxides) in the Skillogalee Dolomite stromatolites. Left-hand column shows images taken in plane polarised light; right-hand column shows images taken under cross-polarised light. Scale bar in **(b)** applies to all images.

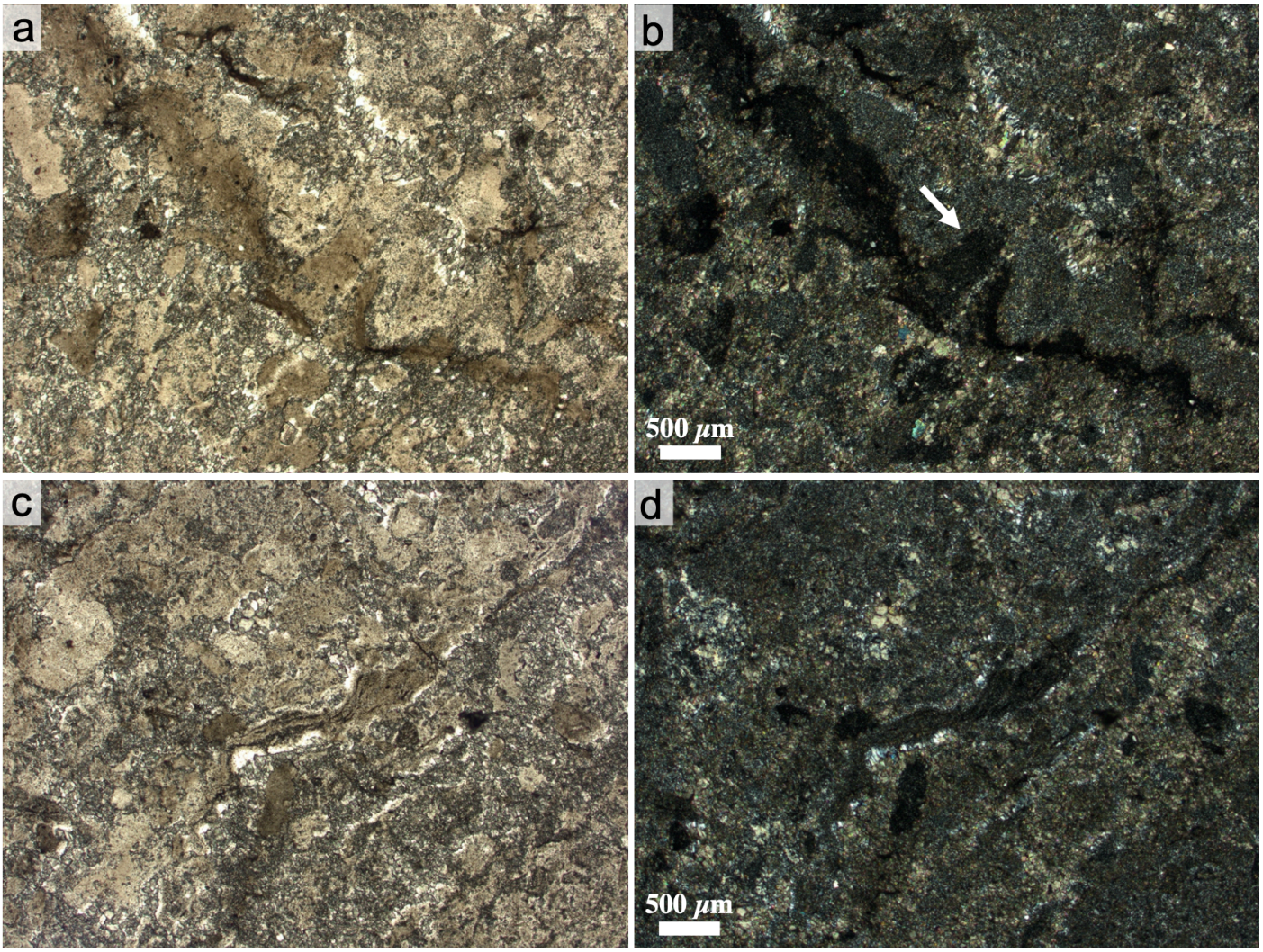

Figure S-6 Optical microscopy observations of organic material-rich laminations in the Skillogalee Dolomite stromatolites. **(a, b)** Organic-rich layer featuring columnar(?) structure. **(c, d)** Non-isopachous, weakly layered organic-rich layer. Plane polarised **(a, c)** and cross polarised **(b, d)** light images are shown. Scale bars in **(b)** and **(d)** apply to **(a)** and **(c)**, respectively. A potential columnar/pseudocolumnar biogenic feature, which may represent the incipient growth of microbial topographic complexity, is arrowed.

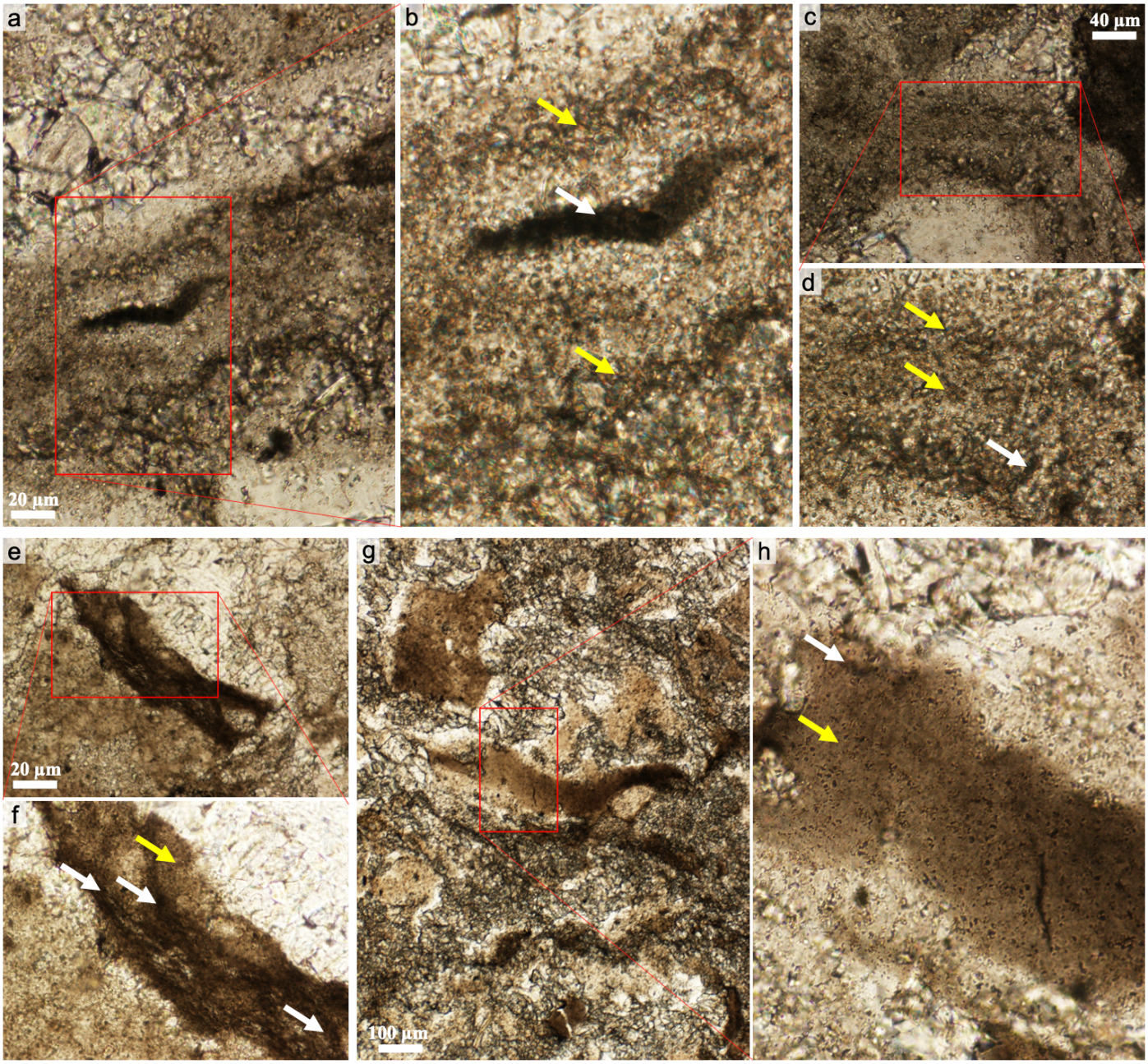

Figure S-7 High-resolution optical microscopy observations of organic laminations and regions of organic staining in stromatolitic laminations. **(a, b)** Laminated organic materials featuring carbonaceous wisps surrounded by pale grey-brown regions of organic staining. **(c, d)** Weakly laminated organic materials surrounded by regions of organic staining. **(e, f)** Laminated organic fragment. **(g, h)** Region of organic staining. White arrows throughout the figure denote primary carbonaceous laminations and fragments; yellow arrows denote regions of organic staining.

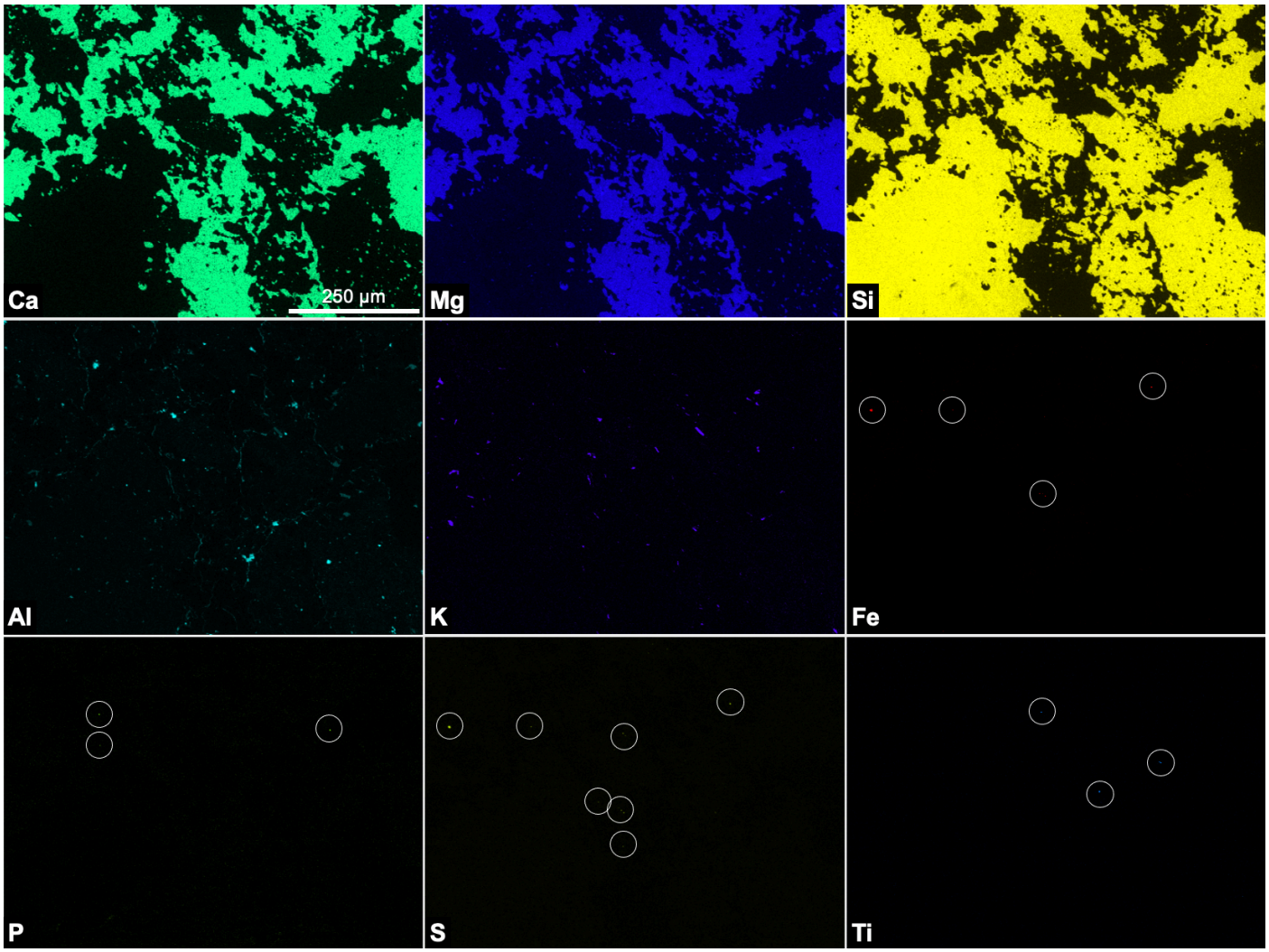

Figure S-8 Complete set of EDS elemental maps corresponding to the region of interest shown in Figure 1c–e.

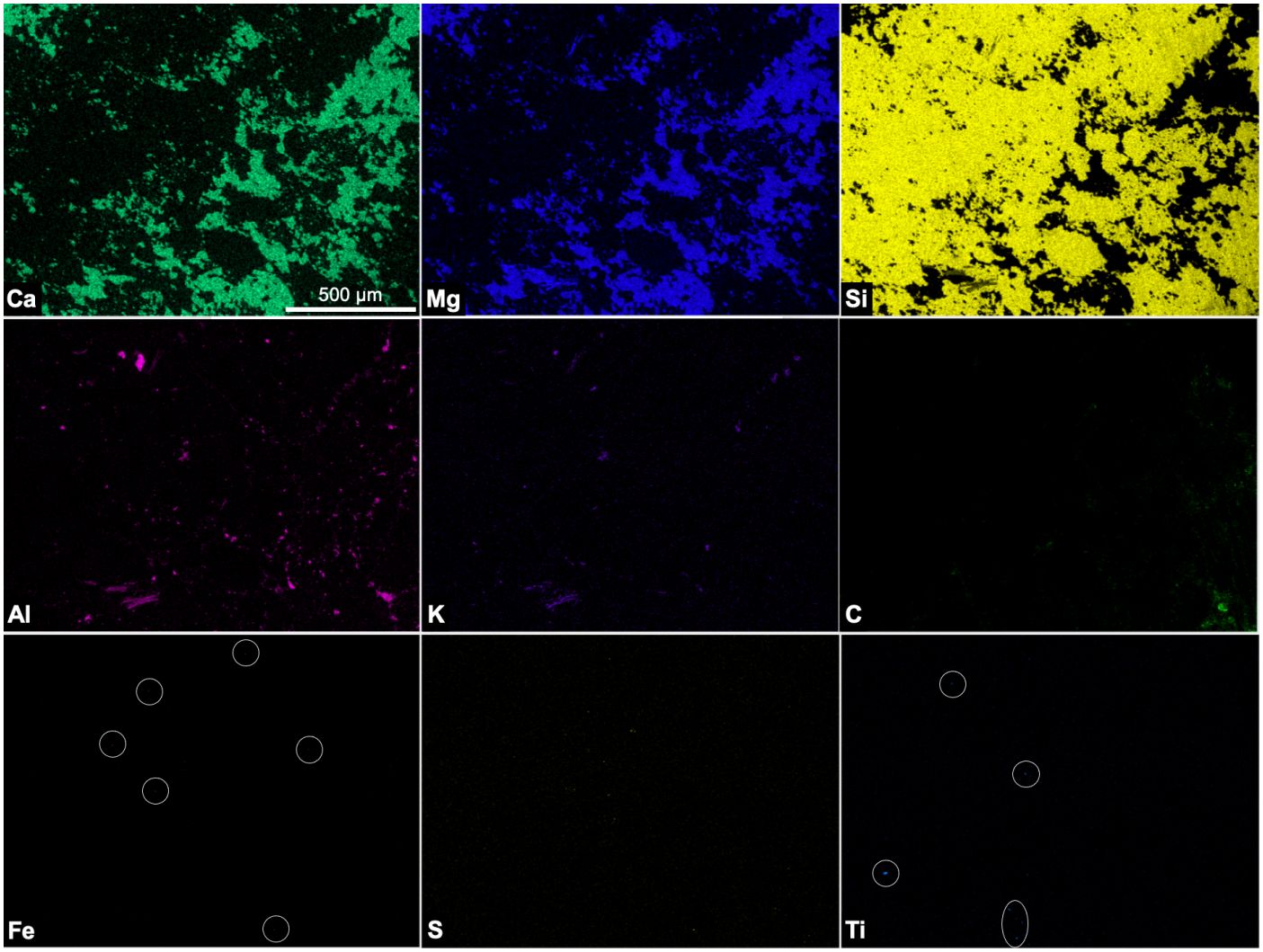

Figure S-9 Complete set of EDS elemental maps corresponding to the region of interest shown in Figure 1f–h.

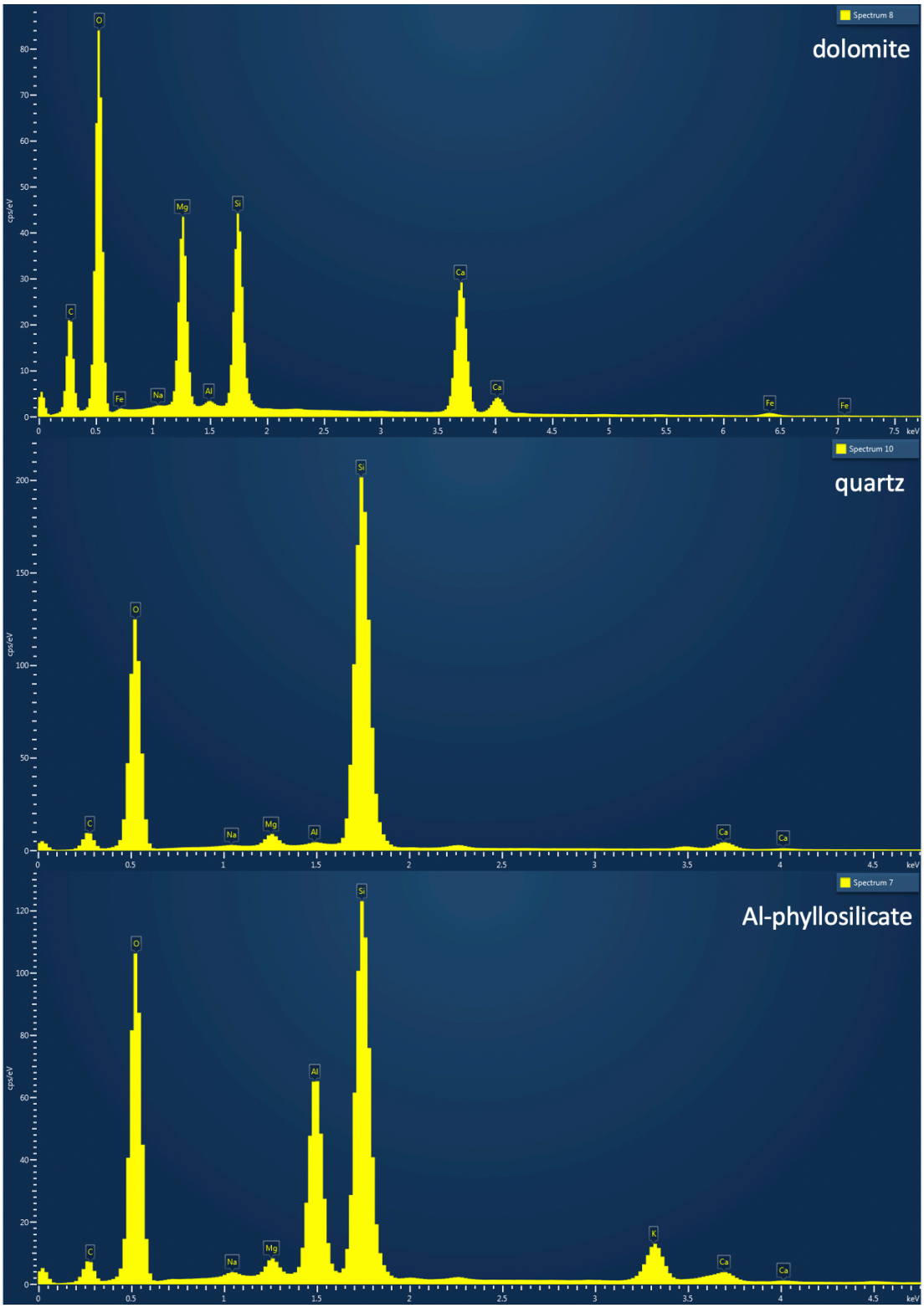

Figure S-10 Representative EDS point analyses of major phases in the Skillogalee Dolomite stromatolites: dolomite, quartz and aluminous phyllosilicate.

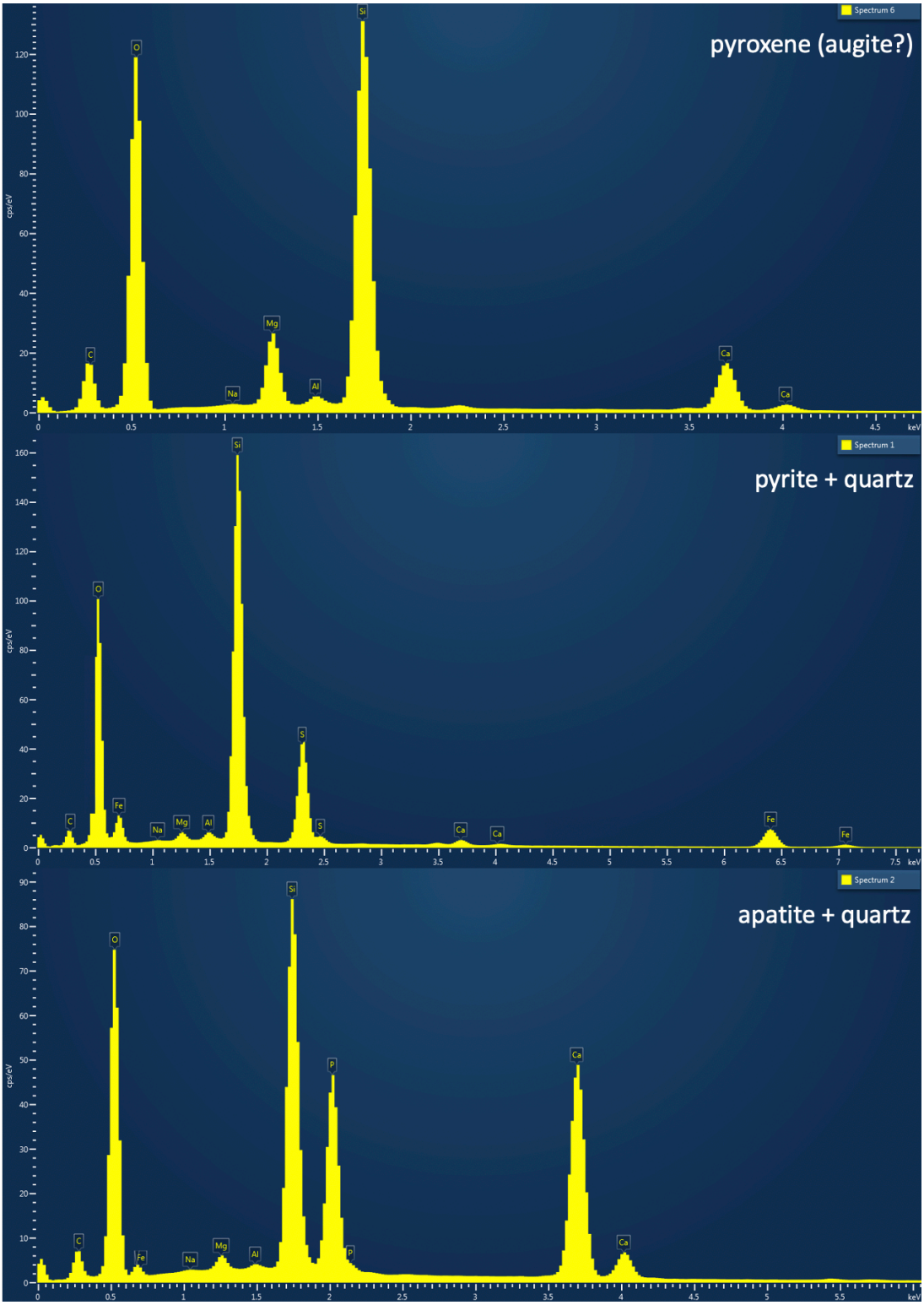

Figure S-11 Representative EDS point analyses of minor phases in the Skillogalee Dolomite stromatolites: pyroxene, pyrite and apatite. Pyrite and apatite occur as micrometric grains and thus the region of analysis features a large contribution from quartz.

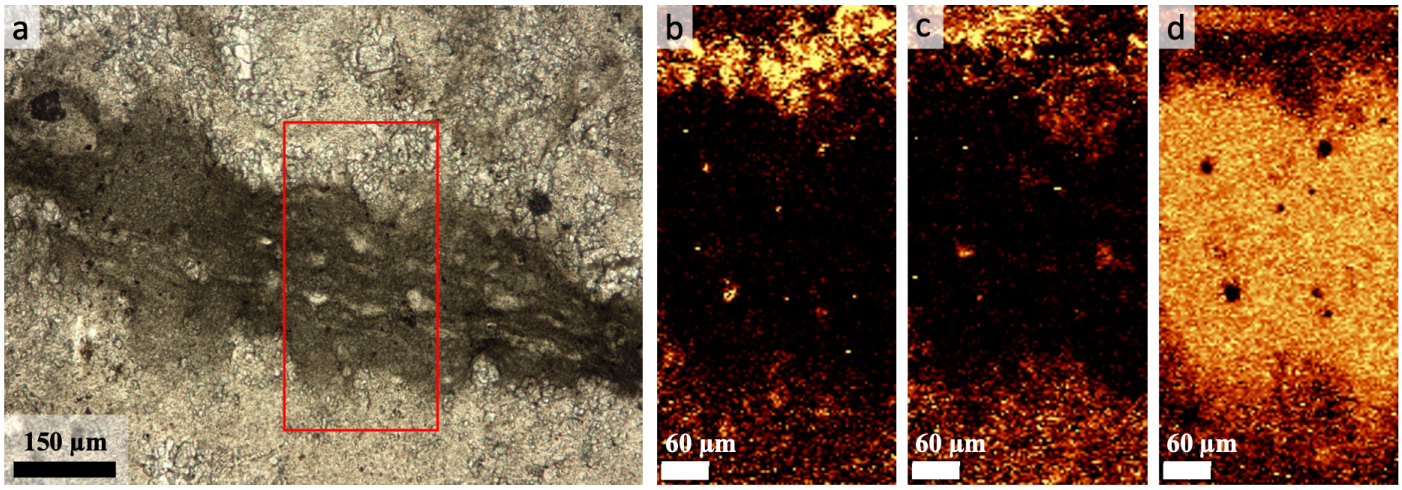

Figure S-12 Raman microspectroscopic mapping of Skillogalee Dolomite stromatolites. **(a)** Optical photomicrograph of organic material-rich layer; red box denotes region of **(b–d)**. **(b–d)** Raman mapping of dolomite, quartz and carbonaceous materials, respectively.

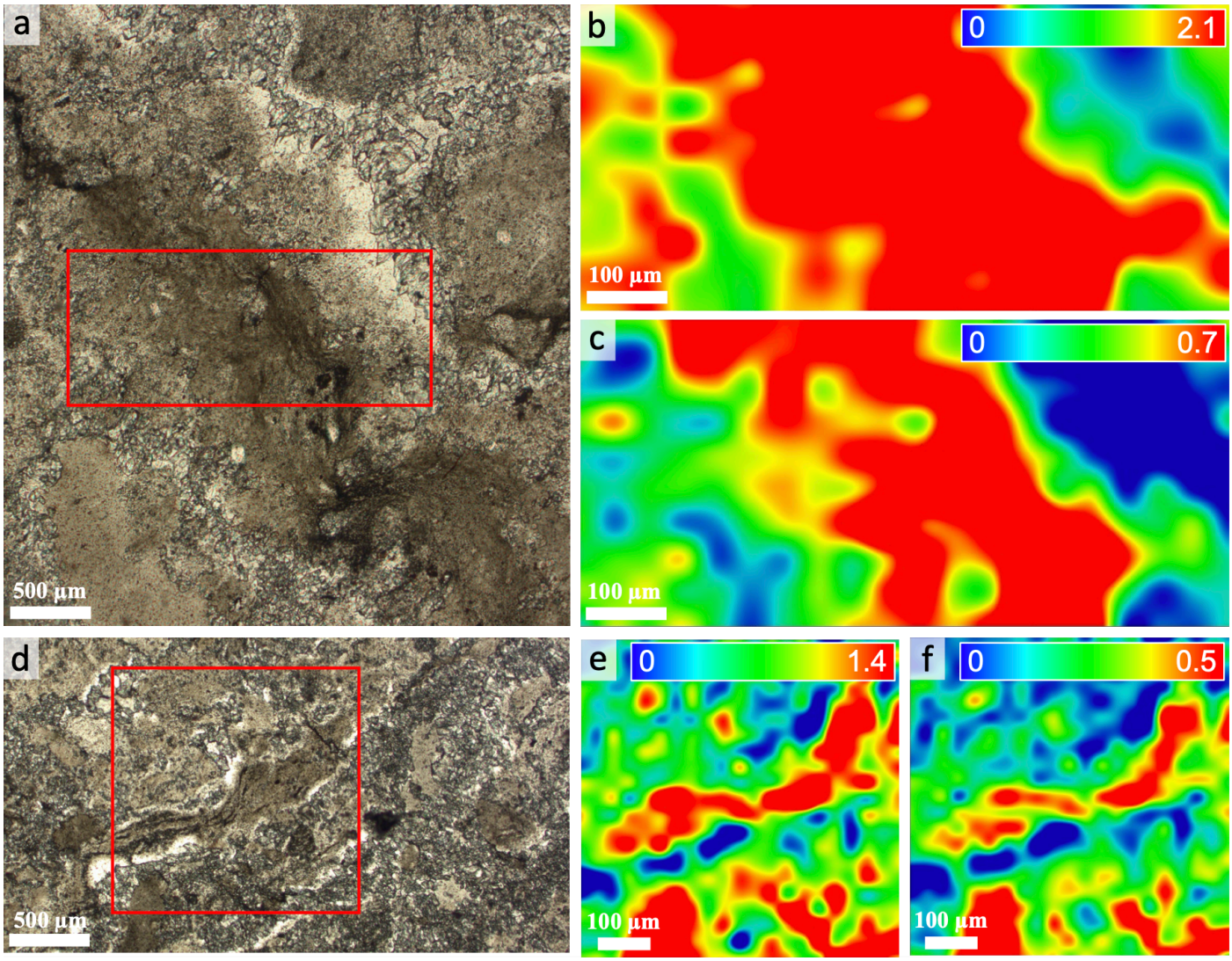

Figure S-13 FTIR microspectroscopic characterisation of organic materials in Skillogalee Dolomite stromatolites. **(a, d)** Optical photomicrographs and FTIR intensity maps of **(b, e)** the C=C band at 1600 cm^{-1} and **(c, f)** the C–H aliphatic band at 2850 cm^{-1}. FTIR maps correspond to red boxes in the optical photomicrographs. Colour scales given in absorbance units.

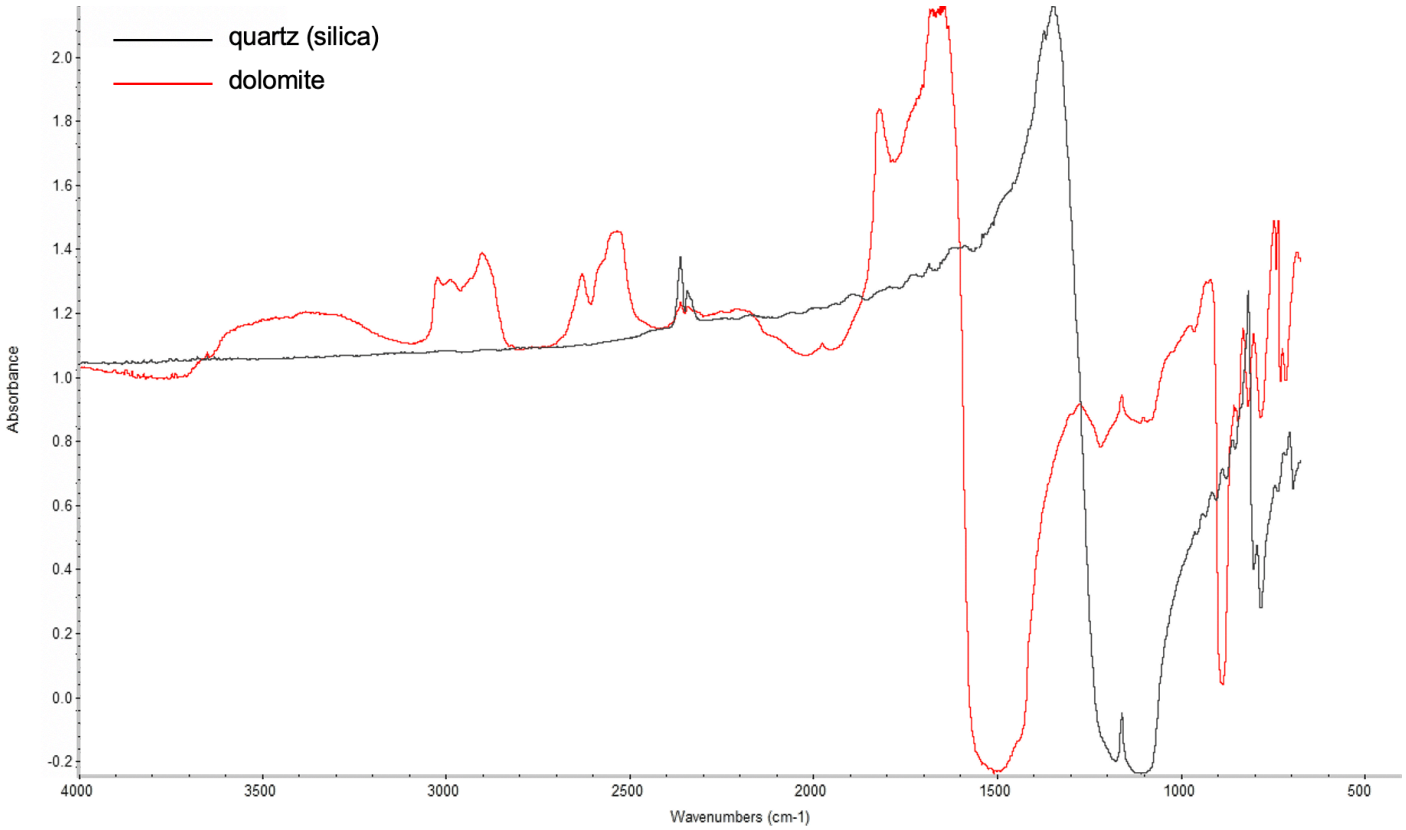

Figure S-14 Representative FTIR spectra acquired in the matrix of the Skillogalee Dolomite stromatolites. Spectra corresponding to both major phases of the matrix, *i.e.* microquartz (silica) and dolomite are shown. Note the absence or complete overprinting of the aliphatic C–H signatures in the 3000–2800 cm^{-1} region. Peaks corresponding to dolomite are as follows: 730, 2520, 2626, 2880, 2985 and 3020 cm^{-1}. Peaks corresponding to quartz are as follows: 793 and 1095 cm^{-1}. Features in both spectra between 2400 and 2100 cm^{-1} arise from atmospheric contributions.

Supplementary Information References

Beyssac, O., Goffé, B., Chopin, C., Rouzaud, J.N. (2002) Raman spectra of carbonaceous material in metasediments: a new geothermometer. *Journal of Metamorphic Geology* 20, 859–871. https://doi.org/10.1046/j.1525-1314.2002.00408.x

Fairchild, I.J., Kennedy, M.J. (2007) Neoproterozoic glaciation in the Earth System. *Journal of the Geological Society* 164, 895–921. https://doi.org/10.1144/0016-76492006-191

Fromhold, T.A., Wallace, M.W. (2012) Nature and significance of the Neoproterozoic Sturtian–Marinoan Boundary, Northern Adelaide Geosyncline, South Australia. *Australian Journal of Earth Sciences* 58, 599–613. https://doi.org/10.1080/08120099.2011.579624

Kouketsu, Y., Mizukami, T., Mori, H., Endo, S., Aoya, M., Hara, H., Nakamura, D., Wallis, S. (2014) A new approach to develop the Raman carbonaceous material geothermometer for low-grade metamorphism using peak width. *Island Arc* 23, 33–50. https://doi.org/10.1111/iar.12057

Preiss, W.V. (1971) *The biostratigraphy and palaeoecology of South Australian Precambrian stromatolites*. Ph.D. Thesis, University of Adelaide.

Preiss, W.V. (2000) The Adelaide Geosyncline of South Australia and its significance in Neoproterozoic continental reconstruction. *Precambrian Research* 100, 21–63. https://doi.org/10.1016/S0301-9268(99)00068-6

Preiss, W.V., Dyson, I.A., Reid, P.W., Cowley, W.M. (1998) Revision of lithostratigraphic classification of the Umberatana Group. *MESA Journal* 9, 36–42.

Virgo, G.M., Collins, A.S., Amos, K.J., Farkaš, J., Blades, M.L., Subarkah, D. (2021) Descending into the "snowball": High resolution sedimentological and geochemical analysis across the Tonian to Cryogenian boundary in South Australia. *Precambrian Research* 367, 106449. https://doi.org/10.1016/j.precamres.2021.106449